ISSN 1392-1207. MECHANIKA. Vol. 31, No. 6, 2025: 524–530

The Effect of the Radius of Curvature on the Joint Strength in Butt-Curved Lap Joints

Şerif ÇİTİL*, Murat PALA**
**Department of mechanical engineering, University of Adıyaman, Adıyaman, Turkey, E-mail: scitil@adiyaman.edu.tr*
***Department of civil engineering, University of Adıyaman, Adıyaman, Turkey, E-mail: pala@adiyaman.edu.tr*
https://doi.org/10.5755/j02.mech.42389

1. Introduction

Structural adhesives are used in almost every field nowadays due to their many advantages [1-2]. Due to the increased prevalence of structural adhesives, the selection of adhesives according to the material to be used and the joint design come to the forefront. Moreover, this necessitates the investigation of the strength of adhesively bonded joints. As choosing a suitable adhesive is required in the adhesively bonded joint, a suitable joint design is also required because the joint type affects the joint strength [3-4]. Especially in cases when the aerodynamic structure is important, it is necessary to apply embedded joint types. In relation to this case, scarf, stepped, and butt joint types come to the fore [5-9]. Adhesives are particularly resistant to shear, rather than tensile force [10]. Shear stresses in adhesively bonded lap joints concentrate in the end regions of the overlap length and cause peel stresses to occur in the same region due to the curvature of adherends and rotations of the joints [11]. In this case, it is necessary to reduce the stress intensity in the end region of the joint. To this end, the joint must be designed to reduce the stress intensity, especially in the end region of the overlap length [12-19]. In embedded joint types, it is possible to increase the surface area of the joint by changing the surface geometries. It is also possible to change the overlap width by changing the surface geometry of the joint model which has the same overlap length and width. In order to reduce the stress intensity at the ends of the joint, especially the overlap width must be increased. Since the geometric parameters of the joint made affect the surface area to which the adhesive is applied, they have an important effect on the joint strength [20-24].

A proper analytical analysis is required to estimate the occurrence of failure in adhesively bonded joints accurately. Failure analyses of the designs with adhesively bonded joints were initially made according to linear elastic assumptions. Since failure occurs in the elastic zone, this solution model was a suitable model for brittle materials, but it was not a sufficient solution model for adhesively bonded joints since most of the adhesives exhibit nonlinear behavior. Later on, elastic-plastic and plastic deformation theories were used in analyses. In the first one of these solution models, the adhesive layer was divided into two zones to be elastic and plastic. With plastic zones found in the end regions with tensile intensity, analyses were performed by considering elastic and plastic zones as separate. In the second solution model, the modulus of elasticity was included as a secant modulus depending on the load. The secant modulus was analyzed by associating total strain with total stress. However, these two solution models could not be implemented since they could not be fully verified. Another approach in the analysis of adhesively bonded joints is the modified von-Mises yield criterion. A system consisting of six non-linear differential equations was derived in this approach, and the analysis was performed iteratively using the finite difference method with variable steps [25]. However, CZM has recently been preferred as a widely used model for adhesives in CZM, which is based on energy principles, the damage situation is examined by utilizing the relationship between shear and normal stresses and displacements. In addition, in CZM, it is accepted that the sample exhibits elastic behavior until the peak of the stress-strain curve, and after reaching the maximum point of the curve, damage begins and fracture occurs. [26]. The geometry of lap joints has a pronounced influence on the distribution of peel stresses. Consequently, a considerable body of research has been devoted to scarf joints and other lap-joint configurations shaped by geometric considerations. In contrast, studies focusing on curved butt-lap joints remain markedly limited. Therefore, the systematic examination of curved butt-lap joints is of substantial significance.

In this research, BCLJs were formed upon aluminum alloy plates with the same overlap length and width and subjected to tensile load. The effects of the created BCLJs on the strength as a result of changing the radius of curvature (RC) were examined. The CZMs based on energy principles were considered for the finite element analysis (FEA) of the lap joints created. Verification tests were performed to verify the finite element solutions.

2. Material and Method

2.1. Material characterization

In this research, in order to create BCLJs, AL2024-T3 plates, which are the most preferred in the field of space and aviation, were used [27]. Two-component DP810 was used as adhesive. To determine the material properties of the adhesive and AL2024-T3 plate, cast samples were prepared and mechanical data were obtained by pulling them at a speed of 1 mm/min on a tensile test device at room temperature. Additionally, the TAST (Thick Adherend Shear Test) model was considered to obtain the shear displacement data of the adhesive [28]. Stress-strain curves in Fig. 1 were shown for the AL2024-T3 plate and adhesive, and their material properties were seen in Table 1 and Table 2.

2.2. Joint fabrication and testing

In order to verify the solutions with finite elements of the butt curved lap joints subjected to tensile load, r = 20, 40 and 60 -mm radii were considered for L_1 = 20 mm overlap length upon aluminum plates, L = 100 mm in length, h = 10 mm in thickness, and w = 25 mm in width. In order

to obtain $t = 0.2$ mm adhesive thickness, curved surfaces with $r_1 = 19.9$, 39.9 and 59.9 -mm radii were formed on plate 1, and curved surfaces with $r_2 = 20.1$, 40.1 and 60.1 -mm radii were formed on plate 2 (Figs. 2, 3). In order to ensure good adhesion between the plate and adhesive in the formed specimens, the plate surfaces were cleaned, and the adhesive was applied on the aluminum plate. The test specimens, to which the adhesive was applied, were obtained by being put in a mold and kept for one day at room temperature. Three specimens were tested for each RC (Fig. 3), the average experimental results are presented graphically in Fig. 9.

The obtained test samples were exposed to a tensile load at a speed of 0.5 mm/min at normal room temperature in a tensile device with a capacity of 100 kN (Figs. 3, 4). In bonded joints adhesively, damages appear on the adhesive, cohesive failure as ASTM-D5573-99 (Figs. 4, 5) [29]. All specimens showed dominant cohesive failure within the adhesive layer, with minor interfacial patterns near the overlap ends.

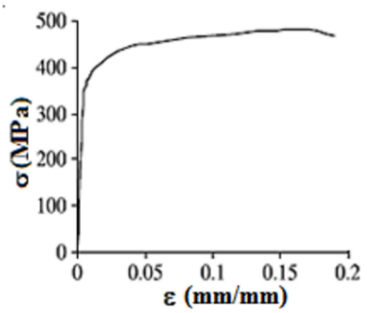

a

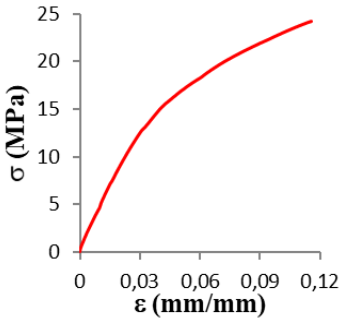

b

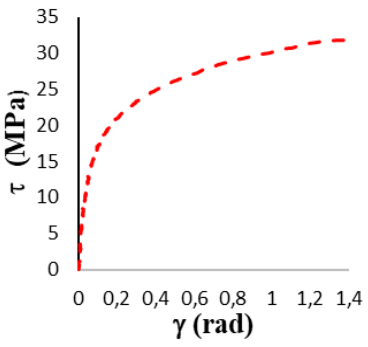

c

Fig. 1 Stress-strain curves: a – AL2024-T3 for normal stress, b – DP 810 for normal stress, c – DP810 for shear stress

Table 1

Material properties of aluminum alloy (2024-T3)

Young's modulus, E, MPa	71875
Poisson's ratio, ν	0.33
Tensile yield strength, σ_y, MPa	361.74
Tensile failure strength, σ_f, MPa	481.9
Tensile failure strain, ε_f, %	0.1587

Table 2

Material properties of DP 810 adhesive

Young's modulus, E, MPa	497.76±28.75
Poisson's ratio, ν	0.35
Tensile yield strength, σ_y, MPa	15.38±3.48
Tensile failure strength, σ_f, MPa	20.07±2.61
Tensile failure strain, ε_f, %	0.078±0.02
Shear modulus, G, MPa	184.35±28.75
Shear yield strength, τ_y, MPa	15.28±4.8
Shear failure strength, τ_f, MPa	29.73±2.02
Shear failure strain, γ_f, %	0.12±0.008
Toughness in tension, G_n^0, N/mm	0.7
Toughness in shear, G_s^0, N/mm	1.9

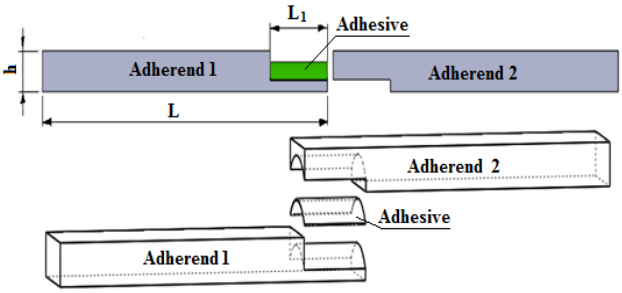

Fig. 2 Geometric representation of BCLJ

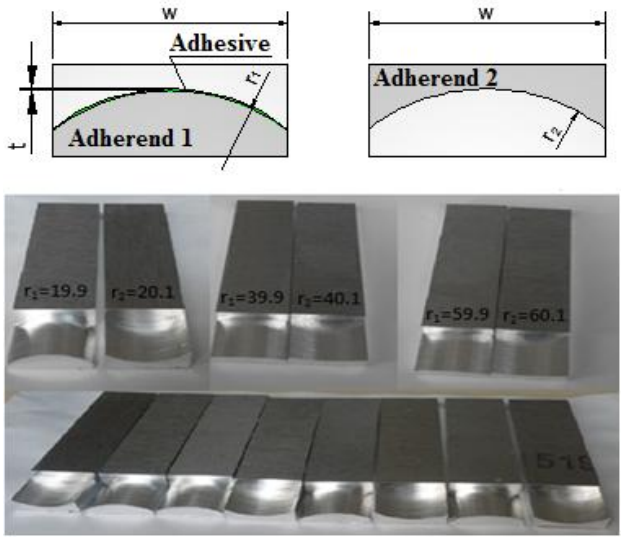

Fig. 3 Test specimens produced in the vertical machining center and their cross-sectional parameters

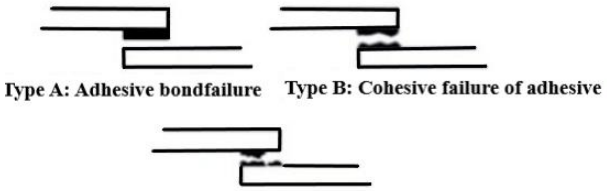

Fig. 4 Cohesive failure in butt-curved lap joints

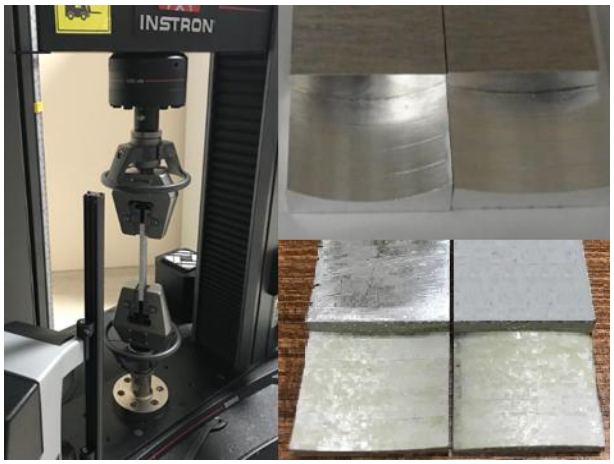

Fig. 5 Conducting experiments in the Instron (5982) tensile device

2.3. Numerical works

For the FEA of the BCLJs, three-dimensional finite element models were created in the Ansys Workbench (Version 15) program [30], and the analysis were presented by mesh detail, boundary conditions and applying load to the created models (Fig 6). The finite element model was modeled as in the tensile test machine in accordance with the realistic conditions and was fixed in the x, y and z directions at point A of Adherend 1. At B point in the end region of Adherend 2 was fixed in the x and y directions, and a tensile load was applied in the z direction. In FEA, the joint is modeled with SOLID186, a 20-node solid element with

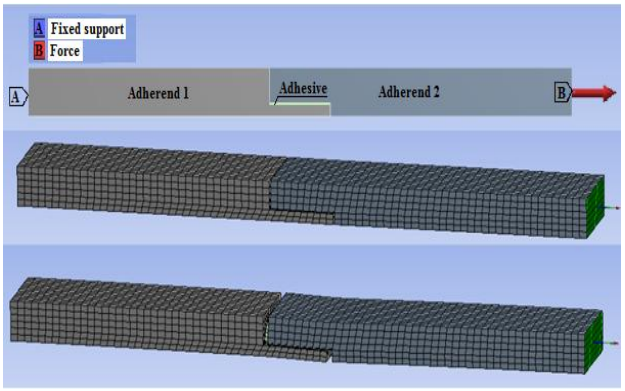

Fig. 6 Boundary conditions and finite element model

displacement degrees of freedom in the x, y, and z directions. SOLID186 is a three-dimensional (3D), higher-order (quadratic) solid element designed for general-purpose structural analyses, providing high accuracy in problems involving geometric and material nonlinearities. To accurately obtain the stress distribution in the adhesive region, a mesh optimization study was conducted. It was observed that when the number of elements was reduced under the same loading conditions, damage did not occur. Therefore, the number of elements was increased until the onset of damage remained unchanged, and the mesh was optimized accordingly. The non-linear material properties of the study were defined by being obtained from Table 1 and Table 2.

The CZM was used for FEA. In the CZM law, a material is considered to be in the elastic region under tensile load up to the maximum point in the stress-strain curve (tensile, shear), and after the maximum point the plastic region begins. [31]. CZM is demonstrated in terms of stress and strain magnitudes that are considered equivalent to shear and tensile states at the material interface that exhibits linear elastic behavior. In the bilinear model of CZM, t_n and t_s are indicated as in the Eq. (1) below [32].

$$t_{n,s} = K_{n,s}\delta_{n,s}\left(1-d_{n,s}\right), \tag{1}$$

$$d_{n,s} = \left\{ \left\{ \left[\frac{\delta_{n,s}-\delta^{0}_{n,s}}{\delta_{n,s}} \right] \left[\frac{\delta_{n,s}-\delta^{0}_{n,s}}{\delta_{n,s}} \right]_{1}^{0} \quad \begin{matrix} \delta^{f}_{n,s} \le \delta_{n,s} \\ \delta_{n,s} \le \delta^{f}_{n,s} \le \delta^{0}_{n,s} \\ \delta^{f}_{n,s} \ge \delta^{0}_{n,s} \end{matrix} \right\}. \tag{2}$$

Here $K_{n,s}$ (K_n at tension, K_s at shear) denotes cohesive stiffness, $d_{n,s}$ (d_n at tension, d_s at shear) denotes the failure parameters for the bilinear cohesive law (here $d_{n,s} = 0$ indicates that the material is in the elastic zone, $d_{n,s} = 1$ indicates that the material failed completely), $\delta^{0}_{n,s}$ denotes the maximum cohesive displacement under tension, $\delta^{f}_{n,s}$ denotes the displacement when the separation is completed, and $\delta_{n,s}$ denotes the maximum displacement along the deformation. In the exponential model of the CZM [33-34], t_n and t_s are expressed as in Eq. (3) and (4)

$$t_n = e\sigma^{max}\Delta_n e^{\left(-\Delta_n\right)} e^{\left(-\Delta_t^2\right)}, \tag{3}$$

$$t_s = 2e\sigma^{max}\frac{\delta_n}{\delta_t}\Delta\left(1+\Delta_n\right)e^{\left(\Delta_n\right)}e^{-\Delta_t^2}. \tag{4}$$

Here, σ^{max} indicates the maximum stress at tension, while Δ_n and Δ_t are stated by Eq. (5)

$$\Delta_{n,t} = \frac{\delta_{n,s}}{\delta^{0}_{n,s}}. \tag{5}$$

In the mixed mode model, t_n and t_s are stated as in Eq. (6)

$$t_{n,s} = K_{n,s}\delta_{n,s}\left(1-d_m\right), \tag{6}$$

$$d_m = \left(\frac{\Delta_{m^{-1}}}{\Delta_m} \right) X \,. \tag{7}$$

Here, for $\Delta_m \leq 0$, $d_m = 0$. For $\Delta_m > 1$, d_m is in the range of $0 < d_m \leq 1$. Furthermore, Δ_m and X are stated as follows:

$$\Delta_m = \sqrt{\Delta_n^2 + \Delta_t^2} \,, \tag{8}$$

$$X = \left(\frac{\delta_{n,s}^f}{\delta_{n,s}^f - \delta_{n,s}} \right) . \tag{9}$$

FEM were analyzed considering to the CZM laws. In the analyses performed with the CZM, t_n and curves were generated by considering Fig. 1 and Table 2 into consideration and were introduced to the ANSYS Workbench program as mixed mode, exponential and bilinear (Fig. 7).

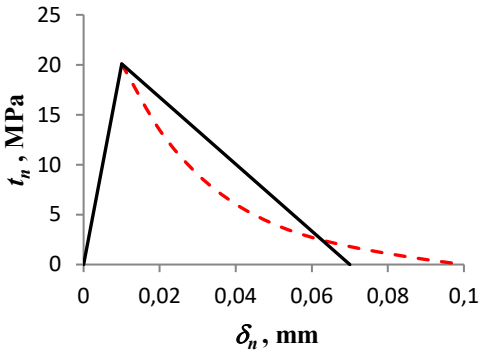

a

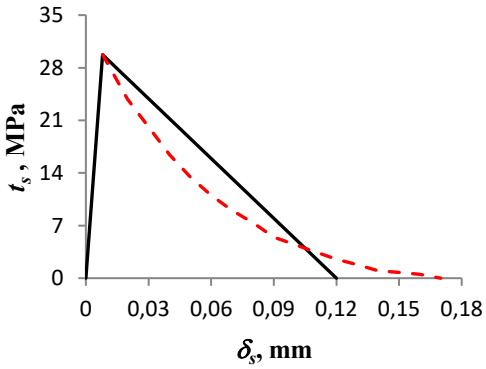

b

Fig. 7 CZM laws for DP810: a – tensile, (t_n), b – shear (t_s)

3. Results and Discussion

3.1. Numerical and Experimental results

The bilinear, exponential and mixed mode solutions of numerical failure loads considering the CZM laws were presented in Fig 7, a, b and c.

When Fig 7, a, b, care examined, the bilinear analyses are observed to give higher, and the exponential solutions are observed to give lower values. Since the experimental results and the bilinear numerical solutions were more compatible, the comparison of the bilinear solutions of the three models were made in Fig 8, d and Fig 7, d demonstrates that the failure loads carried by the specimens increase when the RC decreases. When curved

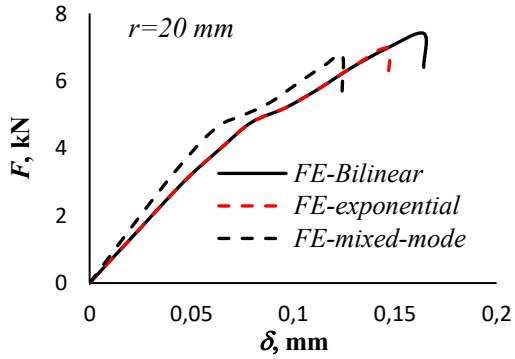

a

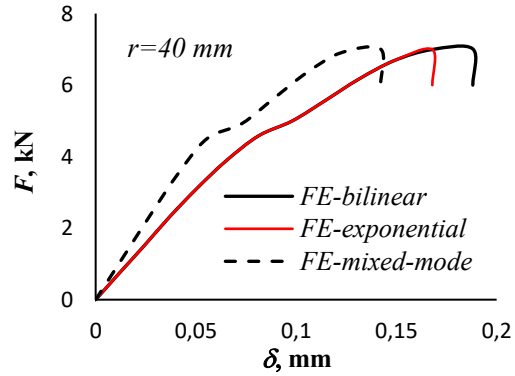

b

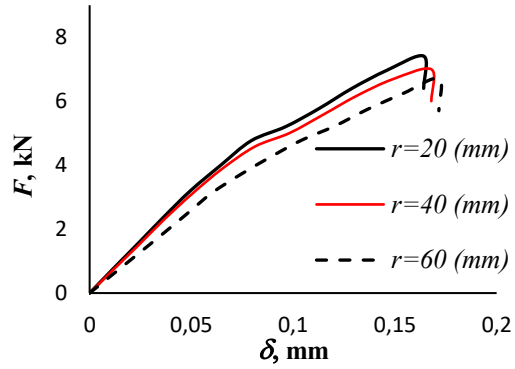

c

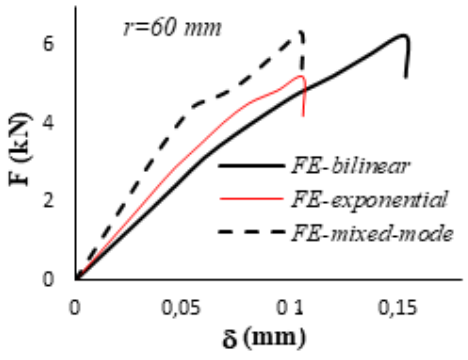

d

Fig. 8 Numerical failure loads considering the CZM laws: a – $r = 20$ mm, b – $r = 40$ mm, c – $r = 60$ mm, d – comparison of failure loads (bilinear)

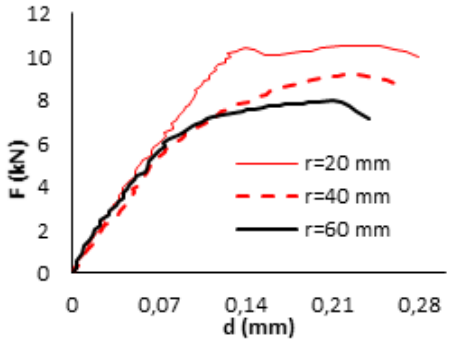

Fig. 9 Experimental failure load results

surfaces are created on the plates of the same dimensions, the failure loads they carry are observed to be affected to a great extent. When numerical results are compared with experimental results (Fig. 9), bilinear solutions are observed to be more compatible.

When the region to which the adhesive is applied on the plates of the same width ($w = 25$ mm) and length ($L = 100$ mm) is examined, the models with the radii of $r_1 = 19.90, 39.90, 59.90$ mm are observed to have the same overlap length ($L_1 = 20$ mm). However, when the radii of $r_1 = 19.90, 39.90, 59.90$ mm are formed on the plates having the same width, the arc lengths (w_1, w_2, w_3) are observed to vary considerably. This is due to the change in the RC. When the radii of curvature and the arc lengths are associated, it is obtained that $w_1 = 32.105$ mm for $r = 20$ mm, $w_2 = 30.53$ mm for $r = 40$ mm, $w_3 = 30.28$ mm for $r = 60$ mm (Fig. 10). This case causes the surface area on which the adhesive is applied to increase as the arc length increases.

Changing the surface area on which the adhesive is applied significantly affects the stress concentration in the overlapping area and the damage loads they carry. Likewise, as the arc length increases, the stress intensity decreases especially in the end parts of the overlap region where the failure starts.

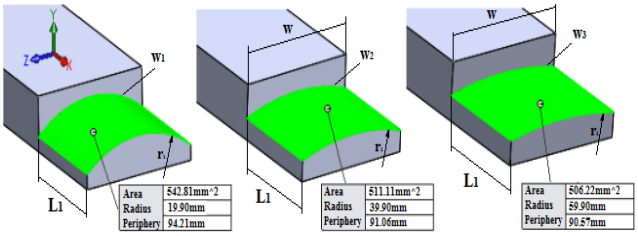

Fig. 10 Arc lengths and surface areas of the BCLJ (w_1, w_2, w_3)

4. Conclusions

BCLJS subjected to tensile load were investigated experimentally and numerically. For this purpose, BCLJS with the same overlap dimensional were formed, and the effect of the RC on strength was investigated. Experimental and numerical results showed that ±10% variations in cohesive strength lead to approximately ±7-12% changes in the predicted failure load, whereas variations in stiffness affect only the initial slope and do not significantly influence the failure load. According to the obtained results, a significant increase in the failure load carried by the adhesively bonded joint was observed as the RC decreased. The arc lengths (w_1, w_2, w_3) were observed to increase as the RC of the adhesively bonded joints with the same width decreased. This situation caused the end regions, where the failure started, to be severely affected, and thus caused the peel stresses to increase and the failure load carried by the specimens to decrease. Furthermore, the surface area, to which the adhesive was applied, decreased as the RC decreased, thus causing the stress intensity of the adhesively bonded joint to increase. While bilinear CZM produced the closest agreement for the tested adhesive and loading state, this may vary for different adhesives or mixed-mode conditions.

References

1. **Barbosa, A. Q.; da Silva, L. F. M.; Abenojar, J.; Figueiredo, M.; Ochsner, A.** 2017. Toughness of a brittle epoxy resin reinforced with micro cork particles: Effect of size, amount and surface treatment, Composites Part B: Engineering 114: 299-310. https://doi.org/10.1016/j.compositesb.2016.10.072.
2. **Sadigh, M. A. S.** 2019. Enhanced Failure Load Bearing in Adhesively Bonded Strap Repairs: Numerical Analysis and Experimental Results, Journal of Failure Analysis and Prevention 19: 182-192. https://doi.org/10.1007/s11668-019-00589-y.
3. **Li, R.; Noda, N.-A.; Takaki, R.; Sano, Y.; Takase, Y.; Miyazaki, T.** 2018. Most suitable evaluation method for adhesive strength to minimize bend effect in lap joints in terms of the intensity of singular stress field, International Journal of Adhesion and Adhesives 86: 45-58. https://doi.org/10.1016/j.ijadhadh.2018.08.006.
4. **Stein, N.; Weißgraeber, P.; Becker, W.** 2015. Model for brittle failure in adhesive lap joints of arbitrary joint configuration, Composite Structures 133: 707-718. https://doi.org/10.1016/j.compstruct.2015.07.100.
5. **Bendemra, H.; Compston, P.; Crothers, P. J.** 2015. Optimisation study of tapered scarf and stepped-lap joints in composite repair patches, Composite Structures 130: 1-8. https://doi.org/10.1016/j.compstruct.2015.04.016.
6. **Li, G.; Lee-Sullivan, P.; Thring, R. W.** 1999. Nonlinear finite element analysis of stress and strain distributions across the adhesive thickness in composite single-lap joints, Composite Structures 46: 395-403. https://doi.org/10.1016/S0263-8223(99)00106-3.
7. **Adin, H.** 2012. The investigation of the effect of angle on the failure load and strength of scarf lap joints, International Journal of Mechanical Sciences 61(1): 24-31. https://doi.org/10.1016/j.ijmecsci.2012.04.010.
8. **Liao, L.; Huang, C.; Sawa, T.** 2013. Effect of adhesive thickness, adhesive type and scarf angle on the mechanical properties of scarf adhesive joints, International Journal of Solids and Structures 50(25-26): 4333-4340. https://doi.org/10.1016/j.ijsolstr.2013.09.005.
9. **Wu, C.; Chen, C.; He, L.; Yan, W.** 2018. Comparison on damage tolerance of scarf and stepped-lap bonded composite joints under quasi-static loading, Composites Part B: Engineering 155: 19-30. https://doi.org/10.1016/j.compositesb.2018.08.031.
10. **Costa-Mattos, H. S.; Monteiro, A. H.; Sampaio, E. M.** 2010. Modelling the strength of bonded butt-joints, Composites Part B: Engineering 41: 654-662. https://doi.org/10.1016/j.compositesb.2010.09.002.

11. **Moreira, R. D. F.; Campilho, R. D. S. G.** 2015. Strength improvement of adhesively-bonded scarf repairs in aluminium structures with important external reinforcements, Engineering Structures 101: 99-110. https://doi.org/10.1016/j.engstruct.2015.07.001.
12. **Marques, E. A. S.; da Silva, L. F. M.** 2008. Joint Strength Optimization of Adhesively Bonded Patches, The Journal of Adhesion 84(11): 915-934. https://doi.org/10.1080/00218460802505275.
13. **Adams, R. D.; Pepiatt, N. A.** 1974. Stress analysis of adhesive-bonded lap joints, Journal of strain analysis 9(3): 185-196. https://doi.org/10.1243/03093247V093185.
14. **Adams, R. D.; Harris, J. A.** 1987. The influence of local geometry on the strength of adhesive joints, International Journal of Adhesion and Adhesives 7(2): 69-80. https://doi.org/10.1016/0143-7496(87)90092-3.
15. **Gleich, D. M.; Van Tooren, M. J. L.; De Haan, P. A. J.** 2000. Shear and peel stress analysis of an adhesively bonded scarf joint, Journal of adhesion science and technology 14(6): 879-893. https://doi.org/10.1163/156856100742942.
16. **Rispler, A. R.; Tong, L.; Steven, G. P.; Wisnom, M. R.** 2000. Shape optimization of adhesive fillets, International Journal of Adhesion and Adhesives 20(3): 221-231. https://doi.org/10.1016/S0143-7496(99)00047-0.
17. **Thoulessa, M. D.; Yang, Q. D.** 2008. Parametric study of the peel test, International Journal of Adhesion and Adhesives 28(4-5), 176-184. https://doi.org/10.1016/j.ijadhadh.2007.06.006.
18. **Da Silva, L. F. M.; Adams, R. D.** 2007. Techniques to reduce the peel stresses in adhesive joints with composites, International Journal of Adhesion and Adhesives 27(3): 227-235. https://doi.org/10.1016/j.ijadhadh.2006.04.001.
19. **Da Silva, L. F. M.; Lopes, M. J. C. Q.** 2009. Joint strength optimization by the mixed-adhesive technique, International Journal of Adhesion and Adhesives 29(5): 509-514. https://doi.org/10.1016/j.ijadhadh.2008.09.009.
20. **Aydin, M. D.; Özel, A.; Temiz, Ş.** 2005. The effect of adherend thickness on the failure of adhesively-bonded single-lap joints, Journal of Adhesion Science and Technology 19(8): 705-718. https://doi.org/10.1163/1568561054890499.
21. **Özel, A.; Aydin, M.; Temiz, Ş.** 2004. The effects of overlap length and adherend thickness on the strength of adhesively bonded joints subjected to bending moment, Journal of Adhesion Science and Technology 18(3): 313-325. https://doi.org/10.1163/156856104773635454.
22. **Özel, A.; Temiz, Ş.; Aydin, M. D.** 2005. Effect of overlap length on durability of joints bonded with a pressure-sensitive adhesive, Journal of Adhesion Science and Technology 19(1): 57-71. https://doi.org/10.1163/1568561053066936.
23. **Adams, R. D.; Harris, J. A.** 1987. The influence of local geometry on the strength of adhesive joints, International Journal of Adhesion and Adhesives 7(2): 69-80. https://doi.org/10.1016/0143-7496(87)90092-3.
24. **Çitil, Ş.; Bozkurt, İ.; Aydın, M. D.** 2019. Experimental and 3D non-linear stress analysis of adhesively bonded pipes with curved-surface lap joints, The Journal of Adhesion 95(5-7): 515-528. https://doi.org/10.1080/00218464.2018.1562922.
25. **Stein, N.; Rosendahl, P. L.; Becker, W.** 2018. Modelling load transfer and mixed-mode fracture of ductile adhesive composite joints, International Journal of Adhesion and Adhesives 82: 299–310 https://doi.org/10.1016/j.ijadhadh.2018.01.013.
26. **Campilho, R. D. S. G.; Banea, M. D.; Neto, J. A. B. P.; da Silva, L. F. M.** 2013. Modelling adhesive joints with cohesive zone models: effect of the cohesive law shape of the adhesive layer, International Journal of Adhesion and Adhesives 44: 48-56. https://doi.org/10.1016/j.ijadhadh.2013.02.006.
27. **Çitil Ş.; Temiz, Ş.; Altun, H.; Özel, A.** 2011. Determination of Mechanical Properties of Double-Strap Adhesive Joints with an Embedded Patch, Journal of Adhesion Science and Technology 25(18): 2555-2567. https://doi.org/10.1163/016942411X580225.
28. ISO 11003-2: 1993. Adhesives – Determination of shear behaviour of structural bonds. Part 2: Thick-adherend tensile-test method. 12p.
29. ASTM D5573-99, 2012. Standard Practice for Classifying Failure Modes in Fiber-Reinforced-Plastic (FRP) Joints.
30. ANSYS Workbench, version 15, 2015. Swanson Analysis Systems, Inc., Houston, Texas.
31. **Jimenez, S.; Duddu, R.** 2016. On the parametric sensitivity of cohesive zone models for high-cycle fatigue delamination of composites, International Journal of Solids and Structures 82: 111–124. https://doi.org/10.1016/j.ijsolstr.2015.10.015.
32. **Alfano, G.; Crisfeld, M. A.** 2001. Finite element interface models for the delamination analysis of laminated composites: mechanical and computational issues, International Journal for Numerical Methods in Engineering 50: 1701-1736. https://doi.org/10.1002/nme.93.
33. **Xu, X. P.; Needleman, A.** 1994. Numerical simulations of fast crack growth in brittle solids, Journal of the Mechanics and Physics of Solids 42(9): 1397-1434. https://doi.org/10.1016/0022-5096(94)90003-5.
34. Ansys HTML Documentation (2008) Cohesive Zone Material (CZM) Model SHARCNet. Available at: https://www.sharcnet.ca/Software/Ansys/17.0/en-us/help/ans_thry/thy_mat11.html (Accessed, 30 July 2007).

Ş. Çitil, M. Pala

THE EFFECT OF THE RADIUS OF CURVATURE ON THE JOINT STRENGTH IN BUTT-CURVED LAP JOINTS

S u m m a r y

In this research, butt curved lap joints (BCLJs) were considered for the aluminum alloy plates exposed to tensile load, and the effect of the radius of curvature (RC) on the joint strength was investigated. For this purpose, butt-curved v joints were formed upon aluminum plates (AL2024-T3), and they were connected using an adhesive (DP810). Finite element analysis joint models were created three-dimensionally, and Cohesive Zone Materials Models (CHZMs) based on energy principles were used to estimate the strength of the adhesively bonded joint. In order to obtain numerical solutions, the parameters of the materials used in the joint model were determined experimentally. Furthermore, verification tests were performed to verify the numerical solutions. From the results obtained, it was understood that the radius of curvature has an important effect on the failure load and stress distributions in butt curved lap joints.

Keywords: adhesives, butt curved lap joint, finite elements, stress analysis

Received July 28, 2025
Accepted December 15, 2025